BENCHMARK STUDY FOR CHARGE DEPOSITION BY HIGH ENERGY ELECTRONS IN THICK SLABS

Insoo Jun
Jet Propulsion Laboratory/California Institute of Technology
4800 Oak Grove Dr.
Pasadena, CA 91109, USA
818-354-7107
Insoo.Jun@jpl.nasa.gov

SUMMARY

The charge deposition profiles created when high energy (1, 10, and 100 MeV) electrons impinge on a thick slab of elemental aluminum, copper, and tungsten are presented in this paper. The charge deposition profiles were computed using existing representative Monte Carlo codes: TIGER3.0 (1D module of ITS3.0) and MCNP version 4B.

The results showed that TIGER3.0 and MCNP4B agree very well (within ~20% of each other) in the majority of the problem geometry. The TIGER results were considered to be accurate based on previous studies. Thus, it was demonstrated that MCNP, with its powerful geometry capability and flexible source and tally options, could be used in calculations of electron charging in high energy electron-rich space radiation environments.

I. INTRODUCTION

Spacecraft are always subjected to radiation environments of various sources that include trapped particles, solar energetic particles and galactic cosmic rays. Space mission design requires (1) knowledge of radiation environments in which the spacecraft will be operating and (2) accurate and reliable radiation transport tools. In the absence of reliable radiation models or transport tools, conservative design to assure reasonable prospects of mission success will generally require more massive shielding of electronic systems or sensors than might otherwise be necessary. Among many phenomena that are possible from space radiation interactions with spacecraft materials, electron charge deposition – either along the particle track or within the bulk of material – is one of the important design issues. It is closely related to internal ESD or bulk charging. Numerous satellite/spacecraft anomalies and failures have been attributed to electron charging problems.[1] Future Jovian missions such as Europa Orbiter will be operating in very intense electron environments in terms of both electron energy and population. Figure 1 illustrates how severe the electron environment is at Jupiter as compared to a typical worst case geosynchronous earth orbit. Therefore, it is apparent that electron charging will be an important design issue for future Jovian missions.

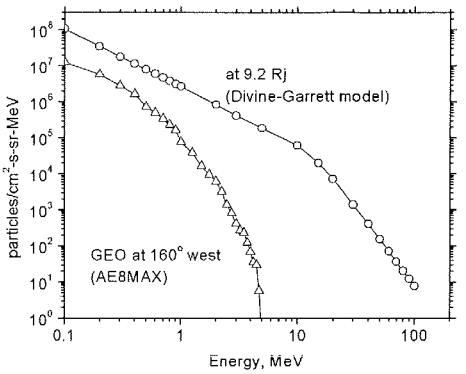

Figure 1. Electron differential spectra for typical GEO and Jovian environments computed based on AE8MAX[2] and Divine-Garrett[3] models, respectively.

This paper particularly addresses high energy (1 to 100 MeV) electron transport in terms of charge-stopping profiles in several representative spacecraft shielding materials (aluminum, copper, and tungsten) with thick slab geometry by using existing electron transport codes (TIGER3.0[4] and, MCNP4B[5]).

TIGER3.0 and MCNP4B are forward codes in that they follow the particles from the source region to the region where the radiation responses are desired. While this approach is advantageous in many applications such as particle beam or reactor configurations, it is computationally inefficient in space applications, which deals with 4-pi omni-directional (isotropic), poly-energetic charged particle radiation sources distributed in space through a complex spacecraft shielding geometry. For spacecraft sized objects, the vast majority of source particles are lost before they reach the

detector. Thus, these forward codes have rarely been used to analyze complex 3D spacecraft geometry due to the excessive run times required.

The main purpose of this paper is to benchmark the MCNP4B code against TIGER3.0, which has been successfully used on many occasions to reproduce the results of electron charging experiments.[6,7] If the MCNP results agree with the TIGER results, it can be concluded that MCNP, which can treat complex geometries and many source distribution/output options, can be used with confidence for high energy space electron charging calculations. Continuous improvement in computer speed will then make calculations practical.

II. PROBLEM SETUP

In order to make the inter-comparison among the codes easier and to focus on the physics used in each code, only the semi-infinite slab geometry was considered in this study. This geometry is implicit in TIGER3.0, while thoughtful geometry modeling is necessary for MCNP4B because it is a 3D code. In order to satisfy the semi-infinite assumption of the geometry, cylindrical slabs with height and radius of $10r_0$ and $100r_0$ were modeled for the MCNP4B calculations, where r_0 is the continuous slowing down approximation (CSDA) ranges of the incident electrons. The broad beam/mono-energetic source electrons were assumed to impinge on one side of the slab with a cosine distribution. The cosine source distribution was used because it is a built-in option in both codes and is easily convertible to an isotropic source problem. Then, the charge depositions were computed in the region from $0.2r_0$ to $0.8r_0$ with $0.025r_0$ intervals. The values of r_0 used in this study are shown in Table 1.

Table 1. CSDA Ranges (g/cm^2) Used in the Calculations[6]

Energy (MeV)	Al	Cu	W
1	0.5546	0.6368	0.7686
10	5.862	6.187	6.211
100	32.12	26.00	19.60

The cut-off energies used are ~0.4% of the source electron energy for TIGER3.0 and 1 keV for MCNP4B. The contribution of lower energy electrons to the total charge deposition is believed to be insignificant.[4] All the final results were normalized to the 1 electron/cm^2 source strength. The number of source particles simulated varies depending on the target material and source electron energy in order to achieve statistical

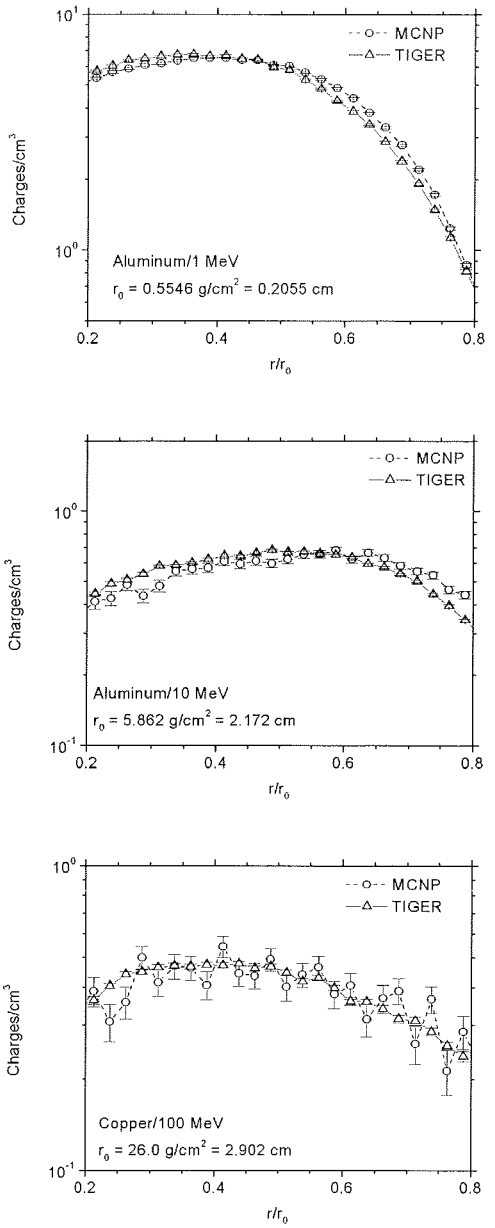

Figure 2. Charge deposition profiles for aluminum target with 1, 10, and 100 MeV source electrons.

uncertainties of the results less than ~10% in the majority of the problem geometry.

III. RESULTS AND DISCUSSION

Figures 2 to 4 summarize the results obtained in this study for aluminum, copper, and tungsten, respectively. They show that TIGER3.0 and MCNP4B agree very well over all energy ranges and material types considered in this study, except in deep regions where the statistical uncertainty of

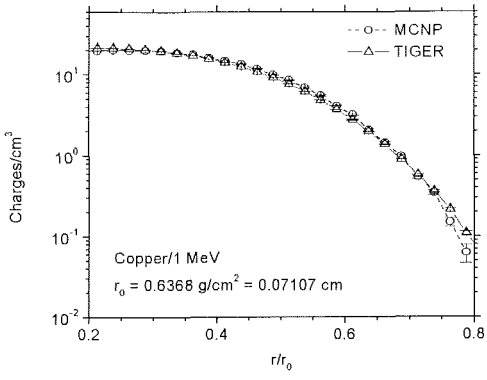

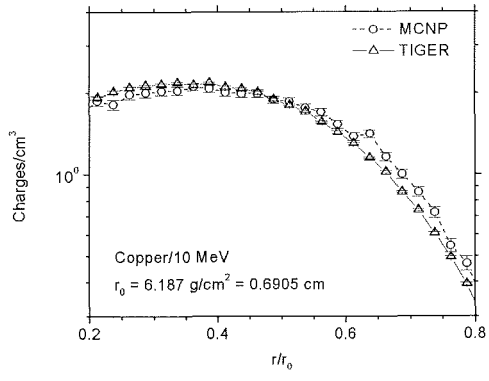

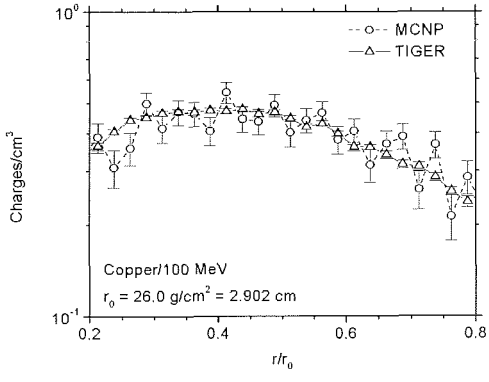

Figure 3. Charge deposition profiles for copper target with 1, 10, and 100 MeV source electrons.

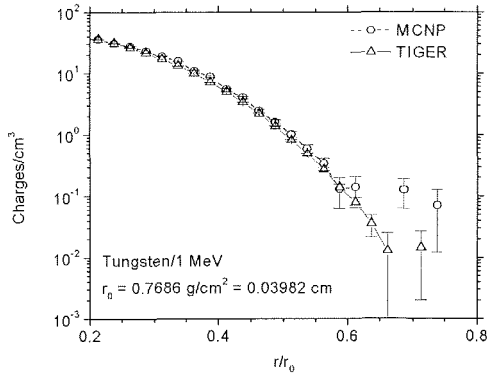

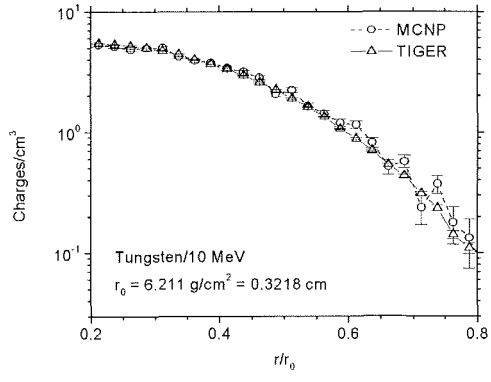

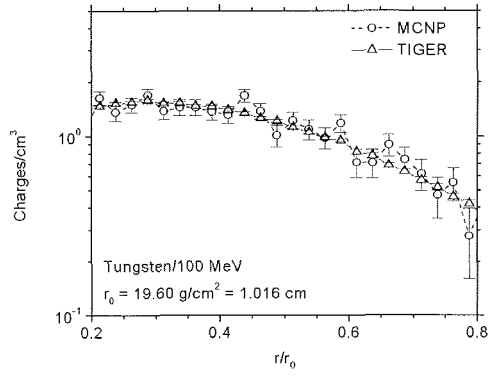

Figure 4. Charge deposition profiles for tungsten target with 1, 10, and 100 MeV source electrons.

the results are large. No effort was taken to improve the uncertainty in these deep regions because of the time and computer CPU constraints. We believe it is sufficient to show that TIGER and MCNP agree each other within 20% in the majority of the problem geometry. The close agreement between TIGER and MCNP4B was expected because the electron physics in MCNP4B is essentially the same as that implemented in TIGER, except for a few minor differences. For example, both codes use multiple scattering algorithms with the Goudsmit-Saunderson theory for angular deflections, the Landau theory of energy loss straggling, the Blunck-Leisegang enhancements of the Landau theory, and the Berger's collisional stopping power. On the other hand, for electron-bremsstrahlung production cross sections, TIGER3.0 uses the data set developed by Seltzer and Berger while MCNP4B relies primarily on the Bethe-Heiter Born-

approximation that has been used in previous versions of TIGER. Figures 5 and 6 compare the collisional and radiative stopping powers, respectively, used in each code for each material considered in this study. As shown, the collisional stopping powers used in each code are almost identical, while the radiative stopping power, which is proportional to the bremsstrahlung production cross sections, is larger for MCNP than for TIGER, especially in the lower energy regions. Therefore, even though the overall agreement for the charge deposition calculations is excellent, the small deviations at the deep regions, aside from the statistical uncertainties, can be attributed to the different bremsstrahlung physics adopted in the two codes. The individual references for the theories mentioned above can be found in the ITS3.0[4] or MCNP4B[5] manuals.

VII. CONCLUSIONS

The charge deposition profiles have been computed using existing electron transport codes for thick elemental targets of aluminum, copper, and tungsten. The transport codes used in this study are TIGER3.0 (1D module of ITS3.0) and MCNP version 4B. The main objective of the study was to compare the MCNP4B results against the TIGER3.0 results, which has been benchmarked extensively against charge stopping experiments. The overall agreement between the two codes came out to be excellent (<20%) in the majority of the problem geometry. With its powerful geometrical modeling capability and flexible source and tally options, MCNP can be very useful for calculations of charging in high energy space electron environments.

ACKNOWLEDGMENTS

The research described in this paper was carried out at the Jet Propulsion Laboratory, California Institute of Technology, under a contract with the National Aeronautics and Space Administration.

REFERENCES

1. H. Garrett and A. Whittlesey, "Spacecraft Charging, An Update," *IEEE Transactions on Plasma Science*, Vol. 28, No. 6, 2017-2028 (2000).

2. J. Vette, "The AE-8 Trapped Electron Model Environment," National Space Science Data Center, WDC-A-R&S 91-24 (1991).

3. N. Divine and H. Garrett, "Charged Particle Distribution in Jupiter's Magnetosphere," *Journal of Geophysical Research*, Vol. 88, No. A9, 6889-6903 (1983).

4. J.A. Hableib et. al., "ITS 3.0: Integrated Tiger Series of Coupled Electron/Photon Monte Carlo Transport Codes," Radiation Safety Information Computational Center (RSICC), Code Package CCC-467, Oak Ridge National Laboratory, (1994).

5. J.F. Briesmeister, the Editor, "MCNP-4B: A General Monte Carlo N-Particle Transport Code, Version 4B," Los Alamos National Laboratory, Report Number LA-12625-M (1997).

6. T. Tabata et. al., "Depth Profiles of Charge Deposition by Electrons in Elemental Absorbers: Monte Carlo Results, Experimental Benchmarks and Derived Parameters," *Nuclear Instruments and Methods in Physics Research B*, Vol. 95, 289-299 (1995).

7. A. Frederickson and S. Woolf, "Electron Beam Current Penetration in Semi Infinite Slabs," *IEEE Transactions on Nuclear Science*, Vol. NS-28, No. 6, 4186-4191 (1981).

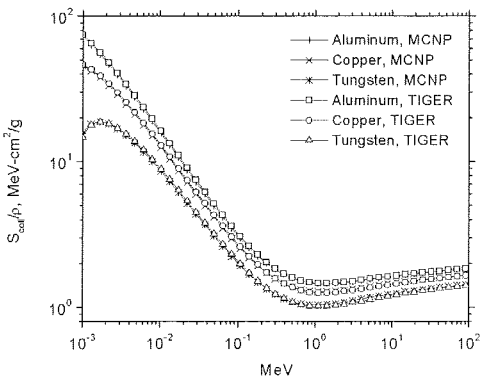

Figure 5. Mass collisional stopping powers used in each code for each material.

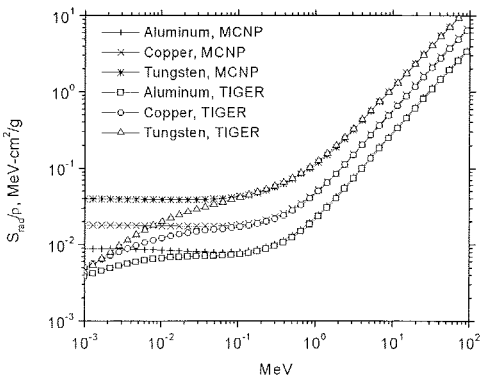

Figure 6. Mass radiative stopping powers used in each code for each material.